The Redox Properties of Ascorbate Peroxidase†

Igor Efimov,‡ Nektaria D. Papadopoulou,‡ Kirsty J. McLean,§ Sandip K. Badyal,‡ Isabel K. Macdonald,‡ Andrew W. Munro,§ Peter C. E. Moody,|| and Emma Lloyd Raven*,‡

Department of Chemistry, University of Leicester, University Road, Leicester, LE1 7RH, United Kingdom, Department of Biochemistry and Henry Wellcome Laboratories for Structural Biology, Henry Wellcome Building, University of Leicester, Lancaster Road, Leicester, LE1 9HN, United Kingdom, and Manchester Interdisciplinary Biocentre, Faculty of Life Sciences, University of Manchester, 131 Princess Street, Manchester, M1 7DN, United Kingdom

Received April 5, 2007; Revised Manuscript Received May 13, 2007

ABSTRACT: Reduction potentials for the catalytic compound I/compound II and compound II/Fe^{3+} redox couples, and for the two-electron compound I/Fe^{3+} redox couple, have been determined for ascorbate peroxidase (APX) and for a number of site-directed variants. For the wild type enzyme, the values are $E^{\circ\prime}$(compound I/compound II) = 1156 mV, $E^{\circ\prime}$(compound II/Fe^{3+}) = 752 mV, and $E^{\circ\prime}$(compound I/Fe^{3+}) = 954 mV. For the variants, the analysis also includes determination of Fe^{3+}/Fe^{2+} potentials which were used to calculate (experimentally inaccessible) $E^{\circ\prime}$(compound II/Fe^{3+}) potentials. The data provide a number of new insights into APX catalysis. The measured values for $E^{\circ\prime}$(compound I/compound II) and $E^{\circ\prime}$-(compound II/Fe^{3+}) for the wild type protein account for the much higher oxidative reactivity of compound I compared to compound II, and this correlation holds for a number of other active site and substrate binding variants of APX. The high reduction potential for compound I also accounts for the known thermodynamic instability of this intermediate, and it is proposed that this instability can account for the deviations from standard Michaelis kinetics observed for most APX enzymes during steady-state oxidation of ascorbate. This study provides the first systematic evaluation of the redox properties of any ascorbate peroxidase using a number of methods, and the data provide an experimental and theoretical framework for accurate determination of the redox properties of Fe^{3+}, compound I, and compound II species in related enzymes.

The catalytic cycle of a heme peroxidase is initiated by oxidation of the Fe^{3+} heme by hydrogen peroxide to form a two-electron-oxidized intermediate, compound I (CI), which contains an oxyferryl iron (Fe^{4+}═O) and either a porphyrin- or, less commonly, a protein-based cation radical. This intermediate is subsequently reduced by the substrate back to the resting (Fe^{3+}) state in two, sequential, one-electron-transfer steps through a second intermediate, compound II (CII), eqs 1−3 (where HS = substrate, $S^{\bullet}$ = one-electron-oxidized form of substrate). Although the involvement of

$$Fe^{3+} + H_2O_2 \xrightarrow{k_1} CI + H_2O \quad (1)$$

$$CI + HS \xrightarrow{k_2} CII + S^{\bullet} \quad (2)$$

$$CII + HS \xrightarrow{k_3} Fe^{3+} + S^{\bullet} + H_2O \quad (3)$$

high-valent heme iron is now well established in the peroxidases and other heme enzymes (*e.g.*, cytochrome *c* oxidase, cytochromes P450), the determination of reduction potentials for the CI/II[1] and CII/Fe^{3+} couples has been a difficult experimental problem. As a result, there are still fairly limited examples of published redox information for these processes (although numerous methodologies have been employed). The first measurements (*1*) were for the CI/CII and CII/Fe^{3+} redox couples in horseradish peroxidase (HRP) and were based on the finding (*2*, *3*) that HRP could be oxidized by K_2IrCl_6 in one-electron steps so that CII was formed directly from the Fe^{3+} enzyme and prior to CI. The same approach was later used (*4*) for HRP and myoglobin in which modified heme derivatives had been introduced, and for *Arthromyces ramosus* peroxidase (*5*). The main drawback of this method is the instability of hexachloroiridate in neutral and alkaline solutions and the difficulty of obtaining reversible equilibria. As an alternative, optically transparent thin layer electrodes (*6*, *7*) offer a more direct way of determining redox potentials (*8*) and this method was first used (*9*, *10*) for HRP using potassium hexachloroiridate as a mediator. A more recent development is the use of cyclic voltammetry to extract the two-electron CI/Fe^{3+} reduction potential in cytochrome *c* peroxidase (*11*). Finally, stopped flow methods have been used to extract CI/Fe^{3+}, CI/CII, and CII/Fe^{3+} reduction potentials for myelop-

† This work was supported by grants from BBSRC (Grant BB/C00602X/1 to E.L.R./P.C.E.M. and studentships to N.D.P. and S.K.B.) and The Leverhulme Trust (Grant RF/RFG/2005/0299 to E.L.R.). A.W.M. thanks the BBSRC and EU for support of research in his laboratory.

* To whom correspondence should be addressed. Tel: +44 (0)116 2297047. Fax: +44 (0)116 252 2789. E-mail: emma.raven@le.ac.uk.

‡ Department of Chemistry, University of Leicester.

§ University of Manchester.

|| Department of Biochemistry, University of Leicester.

[1] Abbreviations: APX, ascorbate peroxidase; rsAPX, recombinant soybean cytosolic ascorbate peroxidase; HRP, horseradish peroxidase; CcP, cytochrome *c* peroxidase; HRP, horseradish peroxidase; CI, compound I; CII, compound II.

10.1021/bi7006492 CCC: $37.00
Published on Web 06/20/2007

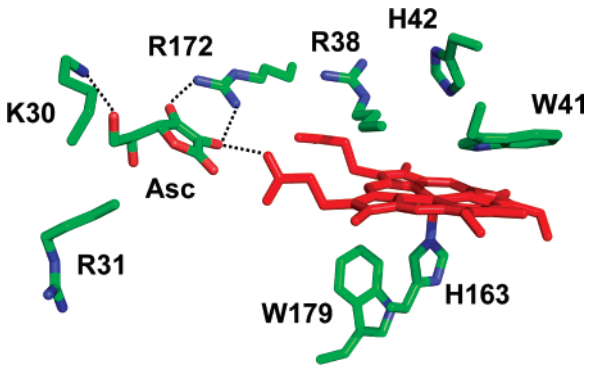

FIGURE 1: Diagram showing the structure of rsAPX (*30*), showing the positions of variants studied in this work. Active site residues (H42 (*32*), R38 and W41 (*16*)) are indicated, and the residues involved in binding of the ascorbate (K30 (*18*), R172 (*18*, *30*)) are also shown. Arg31 is not involved in substrate binding *per se*, but it is directly adjacent to the binding site (*18*). The heme macrocycle is shown in red; Asc = ascorbate. Image was prepared using Pymol (DeLano Scientific).

eroxidase (*12*−*14*) and lactoperoxidase (*15*), and the CI/Fe^{3+} (*12*) reduction potential for eosinophil peroxidase.

In this work, our intention was to establish a complete description of the redox properties for the CI and CII derivatives of ascorbate peroxidase (APX), and to correlate this information with mechanistic data on the substrate binding and heme reduction processes. At the same time, and as part of a more detailed framework of studies aimed at dissecting the thermodynamic and kinetic features that control substrate binding and catalysis in APX, we intended to systematically examine the redox properties of a number of site-directed variants in which key active site residues (R38, H42, W41, Figure 1) and residues involved in substrate binding (R172, K30, K31, Figure 1) have been replaced. The data provide the first assessment of this kind for an ascorbate peroxidase.

MATERIALS AND METHODS

Materials. Recombinant soybean cytosolic ascorbate peroxidase (rsAPX) and the W41 and R38 point mutants were prepared according to published procedures (*16*−*18*). All the substrate binding variants and the H42A, H42A/R38A, and W179F variants were prepared from an expression vector for the pea cytosolic enzyme (rpAPX). Although rsAPX has >90% sequence identity to rpAPX, it contains a conservative substitution at position 30 (K30R), Figure 1. However, the crystal structure of rsAPX shows that R30 overlays closely with K30 in rpAPX (*19*).

Samples of K_3IrCl_6 and K_2IrCl_6 (99.99%) were purchased from Sigma. Aqueous stock solutions of K_3IrCl_6 were stable; aqueous solutions of K_2IrCl_6 were stable when kept concentrated at 5−15 mM with addition of HCl (to 10 mM). Concentrations of these solutions were determined using published absorption coefficients (*1*). Deionized water was used in all experiments.

Redox Potentiometry. Redox titrations were carried out in a glovebox under nitrogen atmosphere, in 100 mM KPi, pH 7.0, 10% glycerol, as described previously (*20*). Pt foil was used as a counter electrode and a saturated calomel as a reference electrode. CII was formed by addition of 1 equiv of both H_2O_2 and ascorbate to the enzyme (9.4 μM) and subsequently reduced to Fe^{3+} by additions of sodium dithionite. The reverse oxidation of Fe^{3+} to CII was carried out by titration with K_2IrCl_6. The UV−visible spectra and the relative potential were recorded after each addition of titrant. Data were fitted to the Nernst equation for a single electron process. The mediators used were phenazine methosulfate (2 μM), 2-hydroxy-1,4-naphthoquinone (5 μM), methyl viologen (0.5 μM), benzyl viologen (1 μM), and ferrocenedicarboxylic acid (2 μM).

Table 1: Reduction Potentials (mV vs NHE) for the Fe^{3+}/Fe^{2+}, CI/Fe^{3+}, CI/II, and CII/Fe^{3+} Redox Couples in rsAPX and Various Site-Directed Variants[a]

	E°/mV			
enzyme	Fe^{3+}/Fe^{2+} [b]	CI/Fe^{3+} [c]	CI/II[d]	CII/Fe^{3+}
rsAPX	−206	954	1156	752[f]
active site variants				
R38A	−239	917	1049	785[g]
R38K	−214	912	1064	760[g]
H42A	−274	nd[e]	nd	820[g]
H42A/R38A	−249	nd	nd	795[g]
W41A	−227	906	1039	773[g]
W179F	−209	904	1053	755[g]
substrate binding variants				
K30A	−203	942	1135	749[g]
K31A	−196	891	1040	742[g]
K30R	−200	913	1080	746[g]
K31R	−205	907	1063	751[g]
K30D	−211	855	953	757[g]
K31D	−225	nd	nd	771[g]
K30A/K31A	−197	806	869	743[g]
K30R/K31R	−192	926	1114	738[g]
R172A	−202	913	1078	748[g]
R172D	−205	903	1055	751[g]
R172K	−198	915	1086	744[g]
K30A/R172A	−202	934	1120	748[g]
K30R/R172K	−178	930	1136	724[g]
K30A/K31A/R172A	−192	770	802	738[g]
K30R/K31R/R172A	−186	923	1114	732[g]

[a] Errors are estimated at ≤5 mV for the experimentally determined values. [b] Determined using the phenosafranin/xanthine/xanthine oxidase method. [c] Determined using the OTTLE method. [d] Calculated potentials derived from CI/Fe^{3+} and CII/Fe^{3+} potentials. [e] Not determined. [f] Determined using redox potentiometry. [g] Calculated using Fe^{3+}/Fe^{2+}reduction potential according to the method of ref *25*.

Thin Layer Spectroelectrochemistry. Reduction potentials for CI/Fe^{3+} were determined using an optically transparent thin layer electrode (OTTLE). The thin layer spectroelectrochemical cell was assembled as described previously (*6*−*8*). Applied potentials were controlled using a potentiostat, and electronic spectra at various applied potentials were recorded using a Perkin-Elmer Lambda 14 spectrophotometer that had been modified to hold the thin layer cell. Gold mesh electrode, platinum grid, and silver wire were used as working, counter, and reference electrodes, respectively. The silver reference electrode was calibrated using the Fe^{3+}/Fe^{2+} potential of the W41A variant (−227 mV, Table 1) measured using phenosafranin/xanthine/xanthine oxidase. The W41A variant was reduced using an OTTLE cell (Supporting Information, Figure 1), and the potential of the silver reference electrode was determined. The same procedure was repeated for rsAPX and produced the shift for Ag/Ag^+ electrode only 8 mV more positive. Enzyme and the mediator K_3IrCl_6 were added to the same concentration of ≈160−200 μM. The absorption coefficient of the mediator is much lower than that of the enzyme; therefore its contribution to the total absorbance was insignificant. To attain equilibration,

the potential was scanned slowly at a rate of 3 μV/s and UV−visible spectra were recorded at 30 min intervals, *i.e.*, every 5.4 mV. The same procedure was repeated for rsAPX, and a similar value was obtained for the reference electrode (−219 mV).

Xanthine/Xanthine Oxidase Method for Determination of Fe^{3+}/Fe^{2+} Reduction Potential. Fe^{3+}/Fe^{2+} reduction potentials for rsAPX and its site-directed variants were determined by simultaneous reduction with a dye of known potential (*21*). This method has the advantage over the OTTLE method in that it allows better equilibria to be obtained because electron exchange occurs in the bulk solution; this means that the method is quicker than the OTTLE method and does not require the correct choice of mediators. The assay contained xanthine (300 μM), xanthine oxidase (50 nM), benzyl viologen (0.2 μM), enzyme (3−4 μM), and the dye phenosafranin ($E^{\circ\prime} = -252$ mV (*22*)). Potassium phosphate buffer (50 mM, pH 7.0) was made oxygen free by using glucose (5 mM), glucose oxidase (50 μg/mL), and catalase (5 μg/mL). Absorbance changes corresponding to reduction of heme were measured at the isosbestic point for phenosafranin (407 nm). Reduction of the dye was measured at 520 nm, where the change due to heme reduction was negligible. In all cases examined, linear Nernst plots for one-electron reduction of heme (25 mV $\ln(E_{ox}/E_{red})$) and two-electron reduction of dye (12.5 mV $\ln(D_{ox}/D_{red})$, where E_{ox}, E_{red} and D_{ox}, D_{red} are the concentrations of oxidized and reduced forms of enzyme and dye, respectively, produced the expected slope of 1 across a wide range of potentials, and the intercept gives a reliable value for $\Delta E^{\circ\prime}$ with an error of ±2 mV.

Data Analysis. UV−visible spectra obtained in all experiments were analyzed using SPECFIT (*23*) for singular value decomposition based on factor analysis. All potentials reported in this paper are given as $E^{\circ\prime}$ (*22*) and are reported versus the normal hydrogen electrode (NHE).

RESULTS

Determination of $E^{\circ\prime}(Fe^{3+}/Fe^{2+})$. The Fe^{3+}/Fe^{2+} reduction potentials were used to calculate CII/Fe^{3+} reduction potentials for APX variants (*vide infra*); therefore we begin with a description of these measurements. Values for $E^{\circ\prime}(Fe^{3+}/Fe^{2+})$ were determined against phenosafranin ($E^{\circ\prime} = -252$ mV (*22*)) using the xanthine/xanthine oxidase method. For rsAPX, the reduction potential was found to be −206 mV, Figure 2 and Table 1. This differs from an early determination on the same enzyme (−159 mV (*24*)). However, we believe the data presented here are more reliable because the derived potential is extracted from considerably more data points (in the previous work the long equilibration times required made it difficult to collect more than a small number of data points) collected over a considerably shorter time (*ca.* 30−60 min compared to about 8−12 h).

Similar families of spectra were obtained for two different categories of site-directed variants: those involved in substrate binding and those at the active site (data not shown). In these experiments, some formation of peroxide (as an oxidation product of glucose) leads to initial oxidation of the Fe^{3+} enzyme to CII (spectra not shown). However, since CII has a very high reduction potential compared to that for phenosafranin and the Fe^{3+}/Fe^{2+} couple, it was quickly reduced back to Fe^{3+} by xanthine oxidase/xanthine without reduction of the dye. The corresponding Fe^{3+}/Fe^{2+} reduction potentials, $E^{\circ\prime}(Fe^{3+}/Fe^{2+})$, are summarized in Table 1 and are used again below for determination of $E^{\circ\prime}$-(CII/Fe^{3+}).

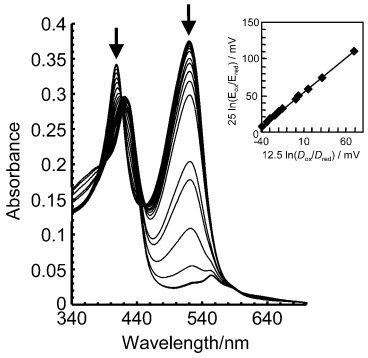

FIGURE 2: Representative family of spectra collected during determination of Fe^{3+}/Fe^{2+} reduction potential in rsAPX (50 mM potassium phosphate, pH 7.0). Arrows indicate direction of absorption changes at various parts of the spectrum during the reductive titration. Inset: the corresponding linear Nernst plot.

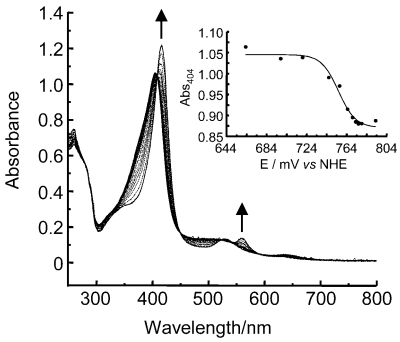

FIGURE 3: Potentiometric titration of rsAPX by K_2IrCl_6, showing spectra recorded during oxidation to CII. Inset: absorbance changes at 404 nm and the corresponding nonlinear fit to the Nernst equation for a one-electron process. Arrows indicate direction of absorption change at different wavelengths during the oxidative titration.

Determination of $E^{\circ\prime}$(CII/Fe^{3+}) for rsAPX. Selected spectra obtained during redox titration of Fe^{3+} rsAPX to CII by K_2IrCl_6 are shown in Figure 3. The reduction to Fe^{3+} was carried out by titration with dithionite. Although the redox process was reversible, satisfactory equilibration was not obtained in a reasonable time for the reductive reaction, and the apparent midpoint potential determined from the reductive reaction was ≈40 mV lower than that obtained for the oxidative titration. Dithionite is a powerful reductant, and we believe that this discrepancy between values for the oxidative and reductive reactions reflects the difficulties associated with establishing equilibration with dithionite in the reductive reaction compared to that for oxidation with K_2IrCl_6. For these reasons, we have used the oxidation data only. Upon oxidation from Fe^{3+} to CII, there is a red shift and an increase in intensity of the Soret band, and bands at 560 and 525 nm in the visible region appear with a clear isosbestic point at 409 nm, Figure 3. These changes are a clear indication of the formation of CII and are consistent with previously published spectra for this intermediate (*17*). From the principle of reversibility (eq 3), and since there is no peroxide present (as in a normal catalytic cycle), we presume that the source of the ferryl oxygen in CII is water.

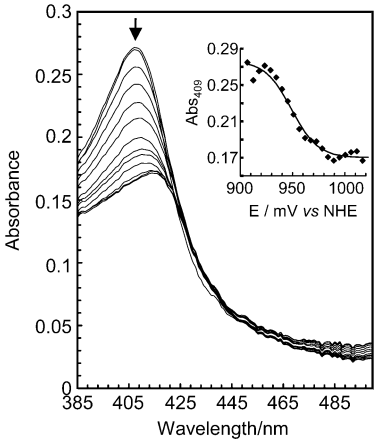

FIGURE 4: Representative family of spectra collected during electrochemical oxidation of rsAPX using an OTTLE cell. The arrow shows the direction of absorbance changes with the increase of potential. Inset: absorbance changes at 409 nm and the corresponding nonlinear fit to the Nernst equation for a two-electron process. $E°'(\text{CI/Fe}^{3+}) = 954$ mV vs NHE.

Changes in absorbance at the Soret maximum, Figure 3 (inset), were analyzed according to a single-electron process, and the calculated value of RT/F = 19 ± 4 mV is close to the expected 25 mV. The midpoint potential, $E°'(\text{CII/Fe}^{3+})$, derived from these data was 752 ± 5 mV vs NHE.

This method was found not to be applicable to any of the site-directed variants examined above because oxidative degradation of the heme (evidenced by lowering of Soret absorbance) was observed during oxidation with K_2IrCl_6.

Determination of $E°'(\text{CI/Fe}^{3+})$. Figure 4 shows a family of spectra for rsAPX collected using the OTTLE method at different applied potentials during anodic scanning (from 700 to 1100 mV vs NHE). The decrease in amplitude of the Soret band is consistent with the formation of CI. During the cathodic sweep, the amplitude of the Soret band was partially (≈30%) recovered, indicating that incomplete rereduction to the Fe^{3+} state occurs. Following this, another positive sweep reproduced the original CI spectrum, though with lower amplitude (data not shown). The Nernst plot, Figure 4 inset, is the best fit to a two-electron oxidation with $E°'(\text{CI/Fe}^{3+}) = 954$ mV vs NHE, Table 1.

Similarly, two-electron reduction potentials, $E°'(\text{CI/Fe}^{3+})$, were also obtained for other variants and are given in Table 1. A representative family of spectra are shown for the R31A variant, Figure 5.

Calculation of $E°'(\text{CI/CII})$ for rsAPX from Experimentally Determined Values of $E°'(\text{CI/Fe}^{3+})$ and $E°'(\text{CII/Fe}^{3+})$. For rsAPX, the measured two-electron reduction potential, $E°'(\text{CI/Fe}^{3+}) = 954$ mV, and one-electron reduction potential, $E°'(\text{CII/Fe}^{3+}) = 752$ mV, were used to calculate $E°'(\text{CI/CII})$ using the relationship $E°'(\text{CI/Fe}^{3+}) = {}^1/_2[E°'(\text{CI/CII}) + E°'(\text{CII/Fe}^{3+})]$ (or $E°'(\text{CI/CII}) = 2E°'(\text{CI/Fe}^{3+}) - E°'(\text{CII/Fe}^{3+})$). The value for $E°'(\text{CI/CII})$ derived in this way was 1156 mV, Table 1.

Calculation of $E°'(\text{CII/Fe}^{3+})$ from Experimentally Determined Values of $E°'(\text{Fe}^{3+}/\text{Fe}^{2+})$. For the variants, we were not able to derive values for $E°'(\text{CII/Fe}^{3+})$ by means of oxidation using K_2IrCl_6 (*vide supra*). An alternative procedure was therefore applied that uses the measured Fe^{3+}/Fe^{2+} potential for each variant to estimate a value for $E°'(\text{CII/Fe}^{3+})$. According to Koppenol and Liebman (*25*) the reduction potential for reduction of CII to Fe^{3+}, eq 4,

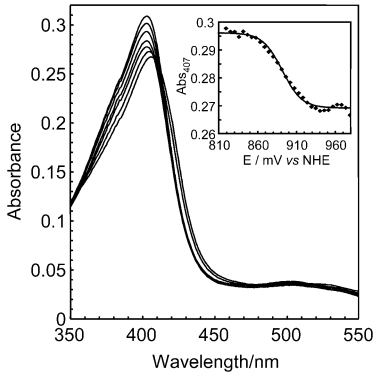

FIGURE 5: Representative family of spectra collected during electrochemical oxidation of R31A using an OTTLE cell. Inset: absorbance changes at 407 nm and a nonlinear fit to the Nernst equation for a two-electron process with $E°'(\text{CI/Fe}^{3+}) = 891$ mV vs NHE.

$$\text{CII} + e^- + 2H^+ \rightarrow Fe^{3+} + H_2O \quad (4)$$

can be calculated from the potentials of the following reactions, eqs 4a−c and eq 5,

$$\text{CII} \rightarrow Fe^{2+} + \text{O(g)} \quad (4a)$$

$$Fe^{2+} \rightarrow Fe^{3+} + e^- \quad (4b)$$

$$\text{O(g)} + 2H^+ + 2e^- \rightarrow H_2O \quad (4c)$$

The reduction potential for eq 4a was calculated (*25*) as $E° = -3.00$ V from gas-phase data for the reaction shown in eq 5,

$$FeO^+(g) \rightarrow Fe^+(g) + \text{O(g)} \quad (5)$$

which assumes that the solvation energies of CII and Fe^{2+} are equal and cancel out. The standard potential for eq 4c is $2E°' = 4.04$ V at pH 7. Expressing eq 4 as the sequence eqs 4a−4c, the following relationship can be derived, eq 6.[2]

$$E°'(\text{CII/Fe}^{3+}) = \text{constant} - E°'(\text{Fe}^{3+}/\text{Fe}^{2+}) \quad (6)$$

The constant in eq 6 can be calculated directly from known pairs of values for $E°'(\text{Fe}^{3+}/\text{Fe}^{2+})$ and $E°'(\text{CII/Fe}^{3+})$, both of which were measured for rsAPX. Thus, from eq 6 one obtains constant = $E°'(\text{CII/Fe}^{3+})_{\text{rsAPX}} + E°'(\text{Fe}^{3+}/\text{Fe}^{2+})_{\text{rsAPX}} = 752 - 206 = 546$ mV. For the purposes of this analysis, we have assumed that this value is independent of the protein environment and is therefore constant for all variants. Hence,

[2] On first glance, it is counter-intuitive that the Fe^{3+}/Fe^{2+} reduction potential appears in eq 6 with a negative sign. Analytically, it follows from eq 4b, which describes *oxidation* (rather than reduction, $Fe^{3+} \rightarrow Fe^{2+}$) of Fe^{2+}, therefore the sign of the potential needs to be reversed. Qualitatively, an explanation was given in ref *4*. In the Fe^{2+} state, the net charge on the iron porphyrin is ∼0, which can be written as $(Fe^{2+}N_4^{2-})$, where N_4^{2-} represents the fact that 2 of the 4 pyrrole nitrogens are negatively charged. Similarly, the Fe^{3+} state has an apparent charge of +1 (denoted as $Fe^{3+}N_4^{2-}$), CII of 0 ($Fe^{4+}O^{2-}N_4^{2-}$), and CI of +1 ($Fe^{4+}O^{2-}N_4^{2-}$)por$^+$. Therefore reduction of CII to Fe^{3+} proceeds with an *increase* of positive charge on iron, which accounts for the negative sign in eq 6 (this is opposite to the change in the charge on reduction of both CI (*i.e.*, from +1 in CI to 0 in CII) and Fe^{3+} (*i.e.*, from +1 in Fe^{3+} to 0 in Fe^{2+})).

Table 2: Summary of Reduction Potentials for APX and Other Peroxidases (*vs* NHE)

enzyme	Fe^{3+}/Fe^{2+}	CI/Fe^{3+}	CI/CII	CII/Fe^{3+}	method	ref
ascorbate peroxidase	−206	954	1156	752	OTTLE, potentiometry	this work
horseradish peroxidase A_2	−190 (*33*)	900	920	880	Ir^{3+}/Ir^{4+} oxidation	*(1)*
horseradish peroxidase C	−278 (*34*)	910	900	920	Ir^{3+}/Ir^{4+}oxidation	*(1, 4)*
		883	898	869	OTTLE	*(9)*
		933	948	918	OTTLE	*(10)*
A. ramosus peroxidase	−183 (*35*)	943	915	982	Ir^{3+}/Ir^{4+} oxidation	*(5)*
cytochrome *c* peroxidase	−194 (*36*)	740			cyclic voltammetry	*(11)*
myeloperoxidase	+24 (*37*)	1160	1350	970	stopped flow	*(12, 14)*
eosinophil peroxidase	nd	1100	nd	nd	stopped flow	*(12)*
lactoperoxidase	−190 (*38*)	1090	1140	1040	stopped flow	*(15)*

the values for $E^{\circ\prime}(CII/Fe^{3+})$ for the variants can be calculated using the measured values of $E^{\circ\prime}(Fe^{3+}/Fe^{2+})$ in each case, eq 7:

$$E^{\circ\prime}(CII/Fe^{3+}) = 0.546\ V - E^{\circ\prime}(Fe^{3+}/Fe^{2+}) \quad (7)$$

This predicted dependence has been observed experimentally (*4*) in separate work on HRP and supports our use of this method here.[3] These values are given in Table 1.

Finally, $E^{\circ\prime}(CI/CII)$ was calculated for each variant from the measured value for $E^{\circ\prime}(CI/Fe^{3+})$ given above and the estimated values for $E^{\circ\prime}(CII/Fe^{3+})$ (using $E^{\circ\prime}(CI/CII) = 2E^{\circ\prime}(CI/Fe^{3+}) - E^{\circ\prime}(CII/Fe^{3+})$). These values are also listed in Table 1.

DISCUSSION

In this paper, our objective was to obtain a complete description of the redox properties of ascorbate peroxidase. To achieve this, several different methods have been used. Redox potentiometry allowed determination of a CII/Fe^{3+} reduction potential for rsAPX: to our knowledge, this is the first time that a redox potential for a heme peroxidase, $E^{\circ\prime}(CII/Fe^{3+})$, has been obtained by direct potentiometric titration. Thin-layer spectroelectrochemistry was used for controlled oxidation of the Fe^{3+} enzyme although, with the exception of rsAPX, only the two-electron reduction potential ($E^{\circ\prime}(CI/Fe^{3+})$) could be directly measured by this method. Separately, Fe^{3+}/Fe^{2+} potentials for rsAPX and numerous site-directed variants were determined using a xanthine/xanthine oxidase assay: this was important for the variants because it allowed estimation of $E^{\circ\prime}(CII/Fe^{3+})$, and hence of $E^{\circ\prime}(CI/CII)$, neither of which were experimentally accessible. Below we describe the implications of these results in the context of the known redox properties of other peroxidase enzymes, and also in terms of our existing understanding of substrate binding and catalysis in APX.

Comparisons with Other Peroxidases. The values for the CI/CII, CII/Fe^{3+}, and CI/Fe^{3+} reduction potentials derived in this work are summarized in Table 2. Also collated in Table 2, for comparison, is a summary of previous measurements of these potentials in other peroxidases. None of these potentials have been reported previously for APX, although computational work (*26*) has estimated $E^{\circ\prime}(CI/CII) = 1080$ mV, which is in agreement with the value reported in Table 1. Broadly, all the peroxidases for which information is available show similar behavior. The most striking similarity is between the measured potentials for APX and myeloperoxidase, in the sense that $E^{\circ\prime}(CI/CII) \gg E^{\circ\prime}(CII/Fe^{3+})$ for both enzymes. This is consistent with the fact that for both proteins compound I is particularly unstable (*27*), a feature which, for APX, was noticed but not rationalized in very early papers (*28*, *29*). This is discussed in more detail below.

Correlations with Mechanistic Data. For APX and all known variants the rate constant for reduction of CI, k_2 (eq 2), is 2−3 orders of magnitude faster than the corresponding rate constant for reduction of CII, k_3 (eq 3). The data in Table 2 help to rationalize this observation. All values for $E^{\circ\prime}(CI/CII)$ are more positive than the corresponding values for $E^{\circ\prime}(CII/Fe^{3+})$ by ≈300−400 mV. For a reaction rate controlled by electron transfer and using a Marcus activation formula with large reorganization energy, λ, theory can predict the relative magnitudes of k_2 and k_3 from the corresponding reduction potentials, eq 8:[4]

$$k_2/k_3 = \exp(\alpha(E^{\circ\prime}(CI/CII) - E^{\circ\prime}(CII/Fe^{3+}))/RT) \quad (8)$$

(where α is the transfer coefficient = 0.5). Using the data in Table 1 for $E^{\circ\prime}(CI/CII)$ and $E^{\circ\prime}(CII/Fe^{3+})$, this equation predicts a value for $k_2/k_3 \approx 10^3$ for rsAPX, which is fairly close to the expected value of $\approx 10^2$ from the published experimental rate constants (*17*, *18*). A similar analysis for the substrate binding variants, in which the mutated residues are not located directly at the active site, can also be used to show that the relationship in eq 8 is also valid, because there is a linear correlation between $RT/\alpha \ln(k_2/k_3)$ *vs* $E^{\circ\prime}(CI/CII) - E^{\circ\prime}(CII/Fe^{3+})$, Figure 6 (in this plot, $\alpha = 1/2$, which is predicted by Marcus theory both for proton and electron transfers). This correlation, Figure 6, spans over 200 mV for these substrate binding variants, and it shows that controlled changes in reduction potential are reflected in the kinetic constants. However, it appears to be valid only for mutations at the substrate binding location (*i.e.*, at ≈10 Å from the active site), which we assume is because the effect on the reduction potential is purely electrostatic for variants which are distant from the heme iron. Accordingly, the active site variants at R38, H42, and W41 would not be expected

[3] Our method of calculation of $\Delta E^{\circ\prime}(CII/Fe^{3+})$ uses eq 7 (*11*), which can be rewritten as $\Delta E^{\circ\prime}(CII/Fe^{3+}) = -\Delta E^{\circ\prime}(Fe^{3+}/Fe^{2+})$. For HRP reconstituted with porphyrins that have been modified at the 2- and 4-vinyl positions, it was shown that the induced changes in pK_3 (where K_3 is the third protonation constant of pyrrole nitrogens of the heme) are related to the variations in potentials as follows: $\Delta E^{\circ\prime}(Fe^{3+}/Fe^{2+}) = -59$ mV ΔpK_3, $\Delta E^{\circ\prime}(CII/Fe^{3+}) = +57$ mV ΔpK_3, and $\Delta E^{\circ\prime}(CI/CII) = -57$ mV ΔpK_3. From these equations, eq 8 follows after exclusion of ΔpK_3.

[4] We have used a ratio of k_2/k_3 in this analysis because the redox potential of the substrate, which may change between different variants, cancels out and does not need to be considered (because of this, attempts to correlate either k_2 or k_3 separately with potential are not successful).

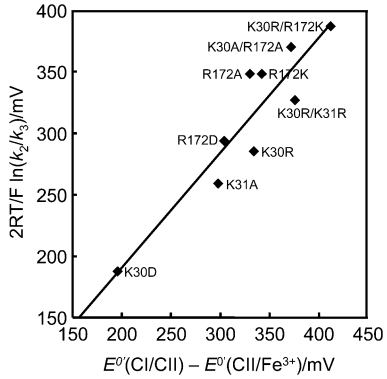

FIGURE 6: Dependence of $2RT \ln(k_2/k_3)$ as a function of $E^{o'}$(CI/CII) − $E^{o'}$(CII/Fe^{3+}) for variants in the substrate binding site. Kinetic constants are from ref *18*.

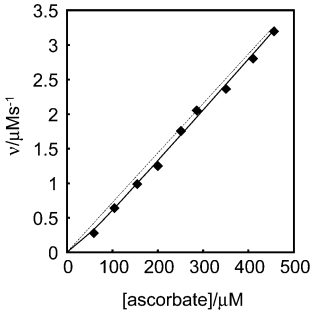

FIGURE 7: Steady-state rate as a function of ascorbate concentration (*17*) (conditions: 25 nM APX, 100 μM H_2O_2 in 50 mM sodium phosphate buffer at 25.0 °C). The solid line represents a fit to eq 9 with $k_3 = 1.5 \times 10^5$ M^{-1} s^{-1}, $k_{2'}/k_2 = 56$ μM. The linear dependence is also indicated (dashed line).

to correlate linearly in the same way because other, non-electrostatic, changes to the active site environment are also introduced as a result of these mutations (see for example ref *16*). This is indeed observed, because no linear correlation, according to Figure 6, could be obtained (data not shown).

Stability of CI and Effect on Steady-State Turnover. As a result of its high reduction potential (1156 mV, Table 1), CI in APX is expected to be unstable. Indeed, kinetic and spectroscopic data from this laboratory and others clearly show that decay of CI to CII occurs very rapidly ($t_{1/2} \approx 20$ ms) (*17*). In contrast, CII has a reduction potential of 752 mV, Table 1, and is therefore expected to be more stable: this is consistent with published spectroscopic data from numerous laboratories (*28*, *29*) which report that CII is stable on a time scale of several minutes.

This difference in stability between the two intermediates also provides some rationalization for the unusual concentration dependence observed during steady-state oxidation of ascorbate. We and others have repeatedly reported that the steady-state oxidation of ascorbate by APXs from various sources does not obey standard Michaelis kinetics (*28*, *29*), and we have shown (*17*) that the most pronounced deviations from Michaelis behavior are at low substrate concentrations, where a sigmoidal dependence of reaction rate on substrate concentration is observed. We originally suggested (*17*) that the presence of more than one substrate binding site for ascorbate may account for the sigmoidal kinetic dependence. However, subsequent structural analyses (*30*) have failed to identify a second binding site, and so if a second site does exist then it certainly has very low affinity for ascorbate.[5] The redox data presented in Table 1 offer an alternative rationalization. Hence, an additional step in the catalytic cycle can now be introduced, eq 2′:

$$\mathrm{CI} \xrightarrow{k_{2'}} \mathrm{CII} \qquad (2')$$

This additional step takes place without ascorbate participation and becomes more significant to the overall reaction rate at low concentrations of the substrate. Consequently, at low concentrations of substrate only one molecule of ascorbate is oxidized in the cycle, whereas two are consumed at high concentrations. This gives rise to a greater than linear acceleration of reaction rate at certain concentrations of substrate (explained in more detail below) and to a deviation from standard Michaelis−Menten behavior. Treatment of the expanded kinetic scheme, eqs 1−3, 2′, using a steady-state approximation (*31*) and assuming $k_3 \ll k_1$, k_2 (which is the case for all APXs examined so far), leads to the following expression, eq 10, for the steady-state rate of substrate oxidation, v:

$$\frac{v}{[\mathrm{E}]} = k_3[\mathrm{HS}]\frac{2k_2[\mathrm{HS}] + k_{2'}}{k_2[\mathrm{HS}] + k_{2'}} \qquad (9)$$

where [E] is the enzyme concentration in the assay and where k_2, $k_{2'}$, and k_3 represent rate constants in eqs 1−3 and 2′ above. In eq 10, only the initial part of the Michaelis−Menten curve is calculated (when [HS] $\ll K_d$): at higher concentrations of substrate (>1 mM) rate saturation takes place (*17*, *18*) and is not analyzed here. From eq 10, at low substrate concentrations [HS] $\ll k_{2'}/k_2$, and it follows that $v/[\mathrm{E}] = k_3[\mathrm{HS}]$; at high substrate concentrations [HS] $\gg k_{2'}/k_2$, and it follows that $v/[\mathrm{E}] = 2k_3[\mathrm{HS}]$, so that the linear slope is doubled at high substrate concentrations. A representative set of data for oxidation of ascorbate fitted to eq 10 is shown in Figure 7, with the corresponding linear part of the Michaelis−Menten dependence also shown. Nonlinearity is clearly present in the observed data compared to the theoretical Michaelis dependence. From the fit to eq 9, the point at which $k_{2'}/k_2 = 56$ μM is the "break point", *i.e.*, the concentration at which 50% of the first reduction step goes through k_2 and the other 50% through $k_{2'}$. At concentrations below the break point, the cycle follows the reaction sequence $k_1 \rightarrow k_{2'} \rightarrow k_3$, and at concentrations above the break point, the cycle is dominated by k_2. APX variants show less deviation from nonlinearity, which can be explained by an alteration in the relative ratios of k_2 and $k_{2'}$ (*i.e.*, an increase in the stability of CI) so that the "break point" concentration is not in the experimental range. The same argument presumably also applies for the steady-state oxidation of guaiacol by APX, which always obeys Michaelis kinetics (*31*, *32*).

[5] We have, however, observed more than one binding orientation for structures of other substrates bound to APX (unpublished data).

ACKNOWLEDGMENT

We thank Professor Grant Mauk and Dr. B. Lue Peter (University of British Columbia) for providing the sticky-backed plastic used for construction of the OTTLE cell.

SUPPORTING INFORMATION AVAILABLE

UV−visible spectra of W41A during reduction using an OTTLE cell, for calibration of the silver electrode. This material is available free of charge via the Internet at http://pubs.acs.org.

REFERENCES

1. Hayashi, Y., and Yamazaki, I. (1979) The oxidation-reduction potentials of compound I/II and compound II/ferric couples of horseradish peroxidase A_2 and C, *J. Biol. Chem. 254*, 9101−9106.
2. George, P. (1952) Chemical Nature of the Secondary hydrogen peroxide compound formed by CcP and HRP, *Nature 169*, 612−613.
3. George, P. (1953) The chemical nature of the second hydrogen peroxide compound formed by CcP and HRP, *Biochem. J. 54*, 267−276.
4. He, B., Sinclair, R., Copeland, B. R., Makino, R., and Powers, L. S. (1996) The structure/function relationship and reduction potentials of high oxidation states of myoglobin and peroxidase, *Biochemistry 35*, 2413−2420.
5. Farhangrazi, Z. S., Copeland, B. R., Nakayama, T., Yamazaki, I., and Powers, L. S. (1994) Oxidation-reduction properties of compounds I and II of *Arthromyces ramosus* peroxidase, *Biochemistry 33*, 5647−5652.
6. Heineman, W. R., Norris, B. J., and Goelz, J. F. (1975) Measurement of Enzyme $E^{o\prime}$ values by Optically Transparent Thin Layer Electrochemical Cells, *Anal. Chem. 47*, 79−84.
7. Reid, L. S., Taniguchi, V. T., Gray, H. B., and Mauk, A. G. (1982) Oxidation reduction equilibrium of cytochrome-b_5, *J. Am. Chem. Soc. 104*, 7516−7519.
8. Taniguchi, V. T., Ellis, W. R., Jr., Cammarata, V., Webb, J., Anson, F. C., and Gray, H. B. (1982) Electrochemical and Spectroelectrochemical Studies of Biological Redox Components, in *Advances in Chemistry Series* (Kadish, K. M., Ed.) pp 51−68, American Chemical Society, Washington DC.
9. Farhangrazi, Z. S., Fossett, M. E., Powers, L. S., and Ellis, W. R. (1995) Variable-temperature spectroelectrochemical study of horseradish peroxidase, *Biochemistry 34*, 2866−2871.
10. Torimura, M., Mochuziki, M., Kano, K., Ikeda, T., and Ueda, T. (1998) Mediator-Assisted Continuous-Flow Column Electrolytic Spectroelectrochemical Technique for the Measurement of Protein Redox Potentials. Application to Peroxidase, *Anal. Chem. 70*, 4690−4695.
11. Mondal, M. S., Fuller, H. A., and Armstrong, F. A. (1996) Direct measurement of the reduction potentials of catalytically active cytochrome *c* peroxidase compound I: voltammetric detection of a reversible, cooperative two-electron transfer reaction, *J. Am. Chem. Soc. 118*, 263−264.
12. Arnold, J., Furtmuller, P. G., Regelsberger, G., and Obinger, C. (2001) Redox properties of the couple compound I/native enzyme of myeloperoxidase and eosinophil peroxidases, *Eur. J. Biochem. 268*, 5142−5148.
13. Boveris, A., Sies, H., Martino, E. E., Docampo, R., Turrens, J. F., and Stoppani, A. O. M. (1980) Deficient metabolic utilisation of hydrogen peroxide in *Trypanosoma cruzi*, *Biochem. J. 188*, 643−648.
14. Furtmuller, P. G., Arnold, J., Jantschko, W., Pichler, H., and Obinger, C. (2003) Redox properties of the couple compound I/compound II and compound II/native enzyme of human myeloperoxidase, *Biochem. Biophys. Res. Commun. 301*, 551−557.
15. Furtmuller, P. G., Arnold, J., Jantschko, W., Zederbauer, M., Jakopitsch, C., and Obinger, C. (2005) Standard reduction potentials of all couples of the peroxidases cycle of lactoperoxidase, *J. Inorg. Biochem. 99*, 1220−1229.
16. Badyal, S. K., Joyce, M. G., Sharp, K. H., Seward, H. E., Mewies, M., Basran, J., Macdonald, I. K., Moody, P. C. E., and Raven, E. L. (2006) Conformational mobility in the active site of a heme peroxidase, *J. Biol. Chem. 281*, 24512−24520.
17. Lad, L., Mewies, M., and Raven, E. L. (2002) Substrate binding and catalytic mechanism in ascorbate peroxidase: evidence for two ascorbate binding sites, *Biochemistry 41*, 13774−13781.
18. Macdonald, I. K., Badyal, S. K., Ghamsari, L., Moody, P. C. E., and Raven, E. L. (2006) The Interaction of Ascorbate Peroxidase with Substrates: a Mechanistic and Structural Analysis, *Biochemistry 45*, 7808−7817.
19. Patterson, W. R., and Poulos, T. L. (1995) Crystal structure of recombinant pea cytosolic ascorbate peroxidase, *Biochemistry 34*, 4331−4341.
20. Papadopoulou, N. D., Mewies, M., McLean, K. J., Seward, H. E., Svistunenko, D. A., Munro, A. W., and Raven, E. L. (2005) Redox and spectroscopic properties of human indoleamine 2,3-dioxygenase and a His303Ala variant: implications for catalysis, *Biochemistry 44*, 14318−14328.
21. Massey, V. (1991) in *Flavins and Flavoproteins* (Curti, B., Ronchi, S., and Zanetti, G., Eds.) pp 59−66, Walter de Gruyter & Co., New York.
22. Clark, W. M. (1972) *Oxidation-Reduction Potentials of Organic Systems*, Robert E. Kreiger Publishing Co., Huntington, NY.
23. Binstead, R. A., and Zuberbuehler, A. D., Spectrum Software Associates, Chapel Hill, NC.
24. Jones, D. K., Dalton, D. A., Rosell, F. I., and Lloyd Raven, E. (1998) Class I heme peroxidases: characterisation of soybean ascorbate peroxidase, *Arch. Biochem. Biophys. 360*, 173−178.
25. Koppenol, W. H., and Liebman, J. F. (1984) The oxidizing nature of the hydroxyl radical. A comparison with the ferryl ion (FeO^{2+}), *J. Phys. Chem. 88*, 99−101.
26. Jensen, G. M. (1998) Energetics of cation radical formation at the proximal active site tryptophan of cytochrome *c* peroxidase and ascorbate peroxidase, *J. Phys. Chem. 102*, 8221−8228.
27. Furtmuller, P. G., Burner, U., Jantschko, W., Regelsberger, G., and Obinger, C. (2000) Two-electron reduction and one-electron oxidation of organic hydroperoxides by human myeloperoxidase, *FEBS Lett. 484*, 139−143.
28. Raven, E. L. (2003) Understanding functional diversity and substrate specificity in haem peroxidases: what can we learn from ascorbate peroxidase?, *Nat. Prod. Rep. 20*, 367−381.
29. Sharp, K. H., Moody, P. C. E., and Raven, E. L. (2003) Defining substrate specificity in haem peroxidases, *Dalton Trans.* 4208−4215.
30. Sharp, K. H., Mewies, M., Moody, P. C. E., and Raven, E. L. (2003) The crystal structure of the ascorbate peroxidase/ascorbate complex, *Nat. Struct. Biol. 10*, 303−307.
31. Dunford, H. B. (1999) *Heme Peroxidases*, John Wiley, Chichester.
32. Lad, L., Mewies, M., Basran, J., Scrutton, N. S., and Raven, E. L. (2002) The role of histidine 42 in ascorbate peroxidase: kinetic analysis of the H42A and H42E variants, *Eur. J. Biochem. 369*, 3182−3192.
33. Yamada, H., Makino, R., and Yamazaki, I. (1975) Effrects of 2,4-substituents of deuteroheme upon redox potentials of horseradish peroxidases, *Arch. Biochem. Biophys. 169*, 344−353.
34. Makino, R., Chiang, R., and Hager, L. P. (1976) Oxidation-reduction potential measurements on chloroperoxidase and its complexes, *Biochemistry 15*, 4748−4754.
35. Battistuzzi, G., Bellei, M., De Rienzo, F., and Sola, M. (2006) Redox roperties of the Fe^{3+}/Fe^{2+} couple in Arthromyces ramosis class II peroxidase and its cyanide adduct, *J. Biol. Inorg. Chem. 11*, 586.
36. Conroy, C. W., Tyma, P., Daum, P. H., and Erman, J. E. (1978) Oxidation-reduction potential measurements of cytochrome *c* peroxidase and pH dependent spectral transitions in the ferrous enzyme, *Biochim. Biophys. Acta 537*, 62−69.
37. Ikeda-Saito, M., and Prince, R. C. (1985) The effect of chloride on the redox and EPR properties of myeloperoxidase, *J. Biol. Chem. 260*, 8301−8305.
38. Ohlsson, P. I., and Paul, G. (1983) The reduction potential of lactoperoxidase, *Acta. Chem. Scand 37*, 917−921.

BI7006492